



## Structural analysis of a posterior stability total knee joint replacement

T. Ingrassia <sup>(a)</sup>, L. Nalbone <sup>(b)</sup>, V. Nigrelli <sup>(a)</sup>, D. Tumino <sup>(c)</sup>, V. Ricotta <sup>(a)</sup>

<sup>(a)</sup> Università degli Studi di Palermo – Dipartimento di Ingegneria Chimica, Gestionale, Informatica e Meccanica

<sup>(b)</sup> Azienda Ospedaliera Universitaria Policlinico Paolo Giaccone di Palermo – Ambulatorio di Ortopedia e Traumatologia

<sup>(c)</sup> Università degli Studi di Enna Kore – Facoltà di Ingegneria ed Architettura

### Article Information

#### Keywords:

Total knee replacement,  
FEM simulation,  
Contact analysis.

#### Corresponding author:

Davide Tumino  
Tel: (+39) 0935536491  
Fax.: (+39) 091484334  
e-mail: davide.tumino@unikore.it  
Address: Facoltà di Ingegneria e  
Architettura, Cittadella Universitaria,  
94100, Enna.

### Abstract

*Aim of this work is to compare two different total knee prostheses that differ in the shape of the Polyethylene (PE) insert, trying to optimize the shape of the best one, in order to reduce the stress peaks.*

*The study procedure has been divided into the following steps. First step has been the three-dimensional shape acquisition of the two prostheses by means of a COMET5 3D scanner. The morphology of two prototypes of the prostheses has been acquired by elaborating multiple Moirè fringe pattern projected on their surfaces. Second step consisted of the manipulation of these data in a CAD module, that is the interpolation of raw data into parametric surfaces, reducing singularities due to the typical scattering of the acquiring system. Third step has been the setting up of FEM simulations to evaluate the prostheses behaviour under typical loading conditions. The CAD model of the prostheses has been meshed into solid finite elements.*

*Different flexion angles configurations have been analysed, the load being applied along the femoral axis. FEM analyses have returned stress fields in the PE insert and, in particular, in the stabilizing cam which function is to avoid dislocation.*

*Last step has been the integrated use of CAD-FEM to modify the shape of the stabilizing cam of the best prosthesis, in order to reduce the stress peaks in the original prosthesis without compromising the kinematics of the joint. Good results have been obtained both in terms of stress and contact pressure peaks reduction.*

## 1 Introduction

Total knee joint replacement allows the patient to restore the full functionality of the knee joint and to overcome arthritic pain. Such a prosthesis consists of femoral and tibial metallic inserts separated by a plastic spacer [1]. Usually, femoral and tibial components are made of titanium, while the plastic insert is made of polyethylene (PE). This PE insert is shaped in a way that dislocation of the joint for high values of flexion angles is avoided [2]. Prolonged use of this prosthesis can cause damaging of the contact surfaces of PE; the creation of debris can lead to infection and, eventually, to a reduced ability of the patient. Load applied to the knee joint during normal activity of the patient has been clinically studied in literature [3-7]. Contact stress distribution in the PE insert follows from the shape of sliding surfaces [8,9]; reducing these stresses can increase the life of prosthesis [10]. Results of numerical analyses can be found [11] for typical posterior-cam stabilized knee prosthesis.

In this work two commercial posterior-stabilized knee joint prostheses have been studied; these are characterised by a different shape of the anti-dislocation system. Numerical comparisons have been performed in terms of contact and equivalent stresses on the plastic insert for both models. Furthermore, geometric modifications of the anti-dislocation element are proposed to enhance the stress distribution and minimize the risk of wearing and fracture damage.

## 2 The knee joint prosthesis

The knee prosthesis is an artificial joint made of metallic alloy and plastic materials, that can replace the damaged knee totally or partially [1]. The total prosthesis consists of three components: the femoral part, the tibial part and the plastic insert that replaces menisci in a healthy knee.

Femoral and tibial components are made of titanium alloy Ti6Al4V, while the plastic insert is made of ultra high molecular weight polyethylene UHMWPE. Fig. 1 shows a standard total prosthesis.



Fig. 1 The total knee joint.

Two different commercial total prostheses are objects of this work: one is produced by Stryker Corp., the other is produced by Tornier. Both of them are considered as

posterior stabilised prosthesis because their shape is made in a way to prevent possible dislocation of the joint due to high flexion angles of the knee joint. Fig. 2 shows the two mentioned prostheses.



**Fig. 2 The Stryker (left) and the Tornier (right) joints.**

Main differences between the two prostheses are related to the plastic insert: in Stryker prosthesis, the PE insert has a central cam element that goes in contact with the mate surface in the femoral part when the flexion angle exceeds a limit value; in Tornier prosthesis, the PE insert has the shape of a hollow guide where a convex surface on the femoral part can slide.

### 2.1 Shape acquisition of the prostheses

To digitally acquire the shapes of the prostheses, a 3D laser scanner COMET 5 has been used. The scanner COMET 5 is composed of a 11 mega-pixel camera, a laser source, a workstation and a software, the COMETPlus, that manages all the data, from the scanning phase to the CAD model exporting. The system has a measuring volume that can vary from 80 to 1000 mm<sup>3</sup>, an accuracy level (depending of the volume) lower than 5 μm and a very reduced acquisition time (about 1 second). The acquisition procedure is here briefly summarised. At first, surfaces to be acquired are sprayed with a mat white colour in order to minimize reflective spurious phenomena. Then a regular fringe pattern is projected on the object surfaces by means of a Laser source. Fringe pattern resulting on the surfaces to be measured is modified according with moiré optical principles [12]. Multiple images have been acquired by rotating the object around a vertical axis. All the fringe patterns have been processed in order to obtain a point-by-point description of the scanned surfaces.

This kind of systems are usually subjected to noise that causes scattering in the acquired points. For this reason, these points have been imported in the Geomagic Studio software where they have been filtered and interpolated into NURBS surfaces [13].

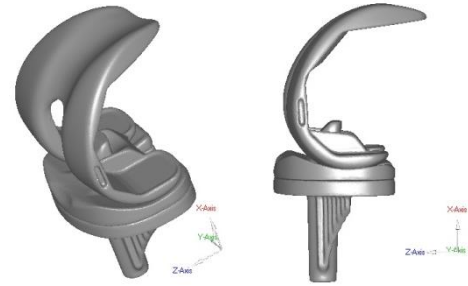


**Fig. 3 Solid model obtained by interpolating surfaces.**

Final step of this process is the conversion of the NURBS surfaces into a CAD solid model, depicted in fig. 3.

### 2.2 Materials

As mentioned before, materials used for these prostheses are titanium alloy Ti6Al4V and high molecular weight polyethylene UHMWPE, both materials are considered as biomaterial because of their high compatibility with human tissues [1]. Main requirements for these materials, and in particular for orthopaedic uses, are:

- Load carrying capability and low stress concentration; loads generated by normal activity of the joint should not be modified by the presence of the prosthesis. Moreover, static, fatigue and creep resistance are of great importance when considering a biomaterial application;
- Kinematics; material used must ensure correct movements of the joint with small friction coefficients and high wearing resistance.

## 3 FEM analysis

3D models of the two prostheses have been imported in the Finite Element (FE) commercial code Ansys Whorlbench. FE models, depicted in figure 4, are meshed with esaedric solid elements.

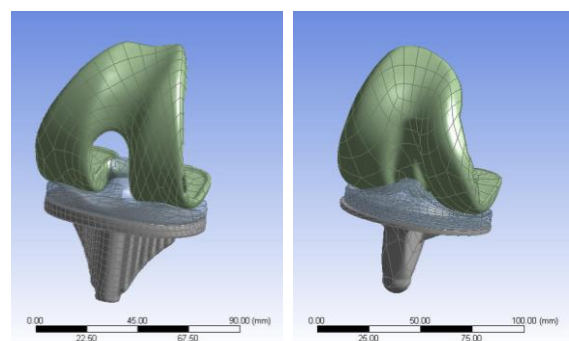


**Fig. 4 CAD models of the two prostheses.**

Table 1 summarises elastic characteristics of the materials used in the models.

	Young Modulus E [MPa]	Poisson ratio	Stress at failure [MPa]
Ti6Al4V	110000	0.34	1140
UHMWPE	2000	0.44	60

Tab. 1 Elastic properties of the materials.

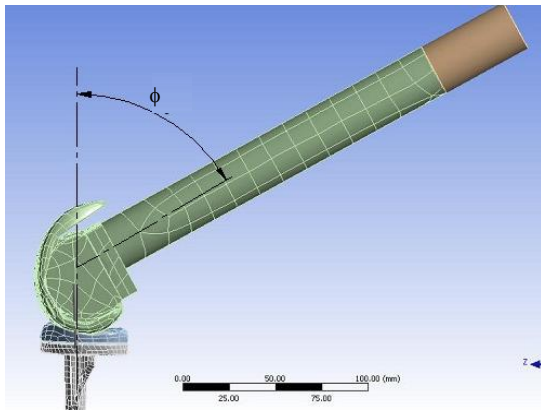


Fig. 5 Flexion angle of the simplified femoral bar.

To apply loads to the joint, the femoral bone has been simulated as a cylindrical bar fixed to the upper component of the knee prosthesis. The axis bar can be positioned in a way to reproduce different flexion angles,  $\phi$ , of the joint, see figure 5.

To reproduce the real working conditions of the prosthesis, two springs have been applied, connecting the tibial to the femoral component. These springs mimic the behaviour of the collateral ligaments, restricting rotations of the femur around its axis. Spring stiffness value has been taken from typical values measured in human ligaments, that is  $K = 34 \text{ N/mm}$ .

External boundary conditions have been applied to the tibial component and to the femoral bar. The tibial component is fixed in all directions, while the femoral bar can only move along and rotate around its axis.

PE insert has been bonded to the tibial component, the same bonding is applied between the femoral bar and the femoral prosthetic component. Friction contact is assumed between the PE insert and the femoral component, with a friction coefficient of 0.01.

A reference load of 500 N is applied on the femoral bar along its axis; different loading conditions are simulated by changing the flexion angle  $\phi$ . In particular, according with experimental tests in literature [4-6], three configurations have been studied:  $\phi = 60^\circ$ ,  $90^\circ$  and  $120^\circ$ . Last value is the maximum flexion angle that can be reached in a normal use of the prosthesis. Different contact regions correspond to each of these angles for both Stryker and Tornier joints [8]. Attention has been paid in evaluating contact and equivalent stresses in the PE insert to be compared with the limit stress of the material. All the obtained results are comparable with other experimental tests [8][9] both in terms of Von Mises and contact stress distribution over the PE insert. All that demonstrates the prostheses reverse engineering process, but also the CAD and FEM modelling phases, are highly reliable.

### 3.1 FEM results – Stryker prosthesis

In the following, contact regions and stress distributions are shown for the PE insert under different flexion angles.

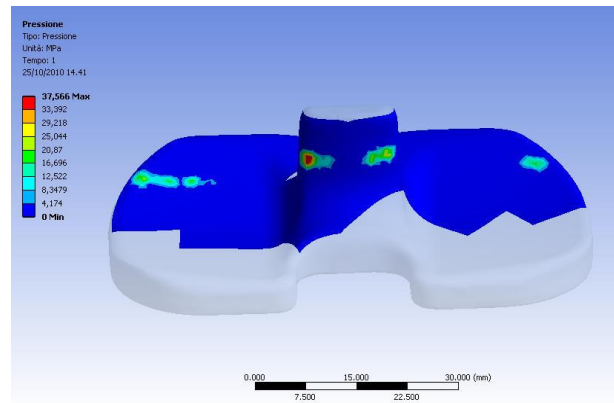


Fig. 6 Contact stress map (Stryker) with  $\phi = 60^\circ$ .

Fig. 6 shows contact regions and contact stress map on the PE insert for  $\phi = 60^\circ$ ; it can be noticed that contact is restricted to external areas of the plate and to the central cam, where maximum peaks are present. In fig. 7, the distribution of the Von Mises stress is depicted for the same case of  $\phi = 60^\circ$ .

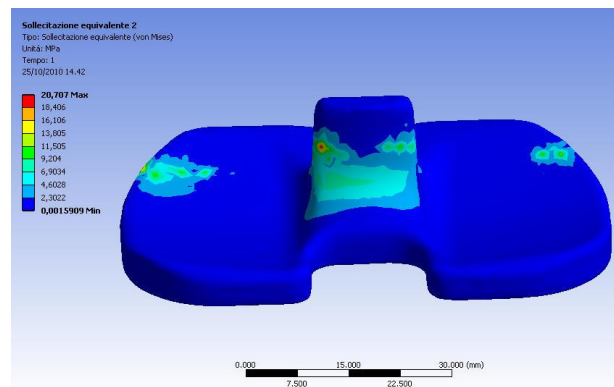


Fig. 7 Von Mises stress map (Stryker) with  $\phi = 60^\circ$ .

Fig. 8 shows contact stress map for  $\phi = 90^\circ$ . Contact areas on the plate are different with respect to the case of  $\phi = 60^\circ$ , and contact stress peaks on the central cam can reach higher values. Similar considerations can be done for equivalent stresses in fig. 9.

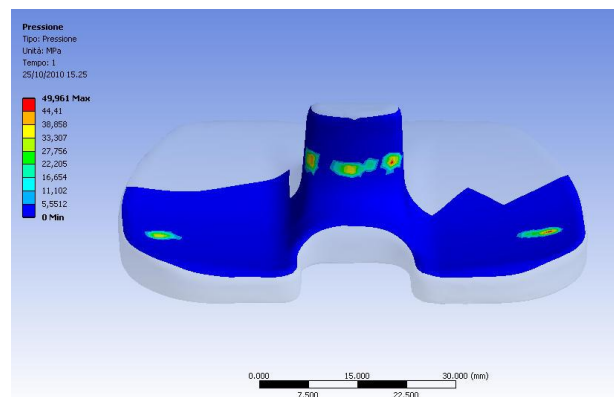


Fig. 8 Contact stress map (Stryker) with  $\phi = 90^\circ$ .

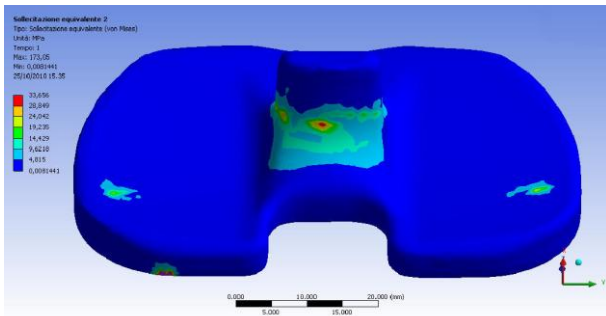


Fig. 9 Von Mises stress map (Stryker) with  $\phi = 90^\circ$ .

Last case is related to  $\phi = 120^\circ$ . Fig. 10 shows that most of the contact load is applied at the top of the central cam and peak values are quite high. Also concerning equivalent stress (fig. 11) the map shows that the cam is severely stressed.

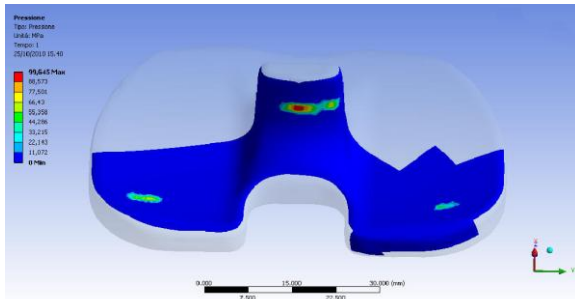


Fig. 10 Contact stress map (Stryker) with  $\phi = 120^\circ$ .

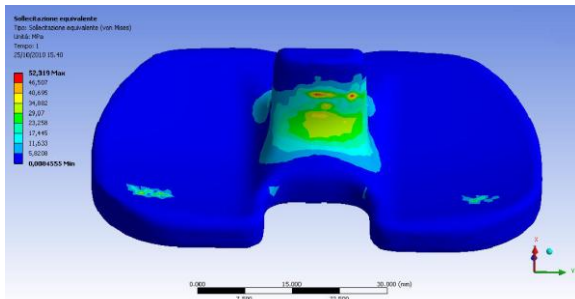


Fig. 11 Von Mises stress map (Stryker) with  $\phi = 120^\circ$ .

### 3.2 FEM results – Tornier prosthesis

Same loading conditions have been applied to the Tornier prosthesis. In the following figures, contact regions and stress distributions are shown for the PE insert under different flexion angles. Figures 12 and 13 are related to  $\phi = 60^\circ$ . Contact is distributed over the plate in two symmetric areas, the central guide is unloaded.

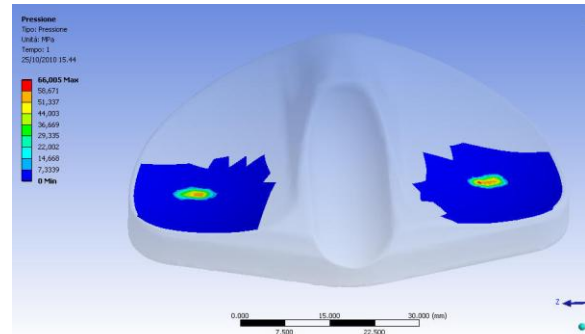


Fig. 12 Contact stress map (Tornier) with  $\phi = 60^\circ$ .

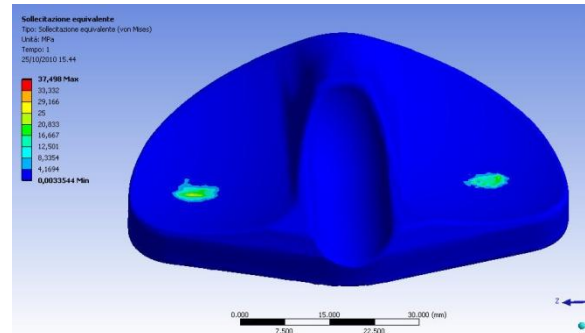


Fig. 13 Von Mises stress map (Tornier) with  $\phi = 60^\circ$ .

Figures 14 and 15 are related to  $\phi = 90^\circ$ . Contact is concentrated at the end of the central guide where a stress peak is present, both in terms of contact and equivalent stress.

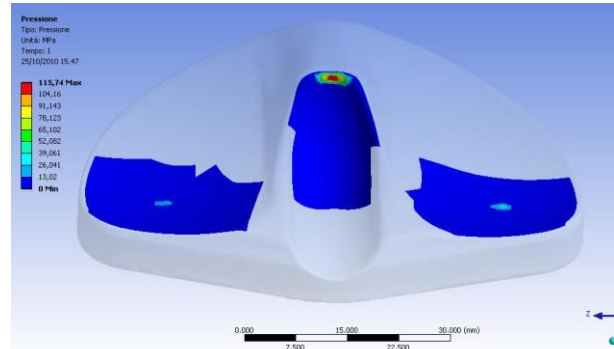


Fig. 14 Contact stress map (Tornier) with  $\phi = 90^\circ$ .

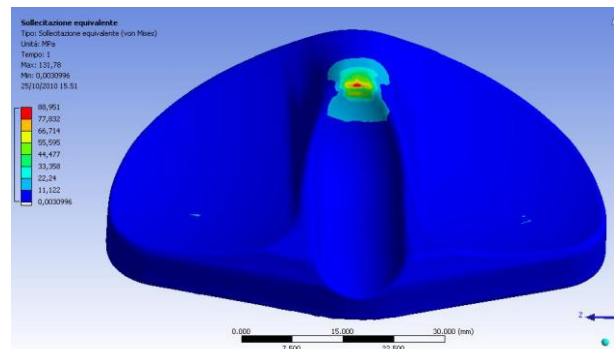


Fig. 15 Von Mises stress map (Tornier) with  $\phi = 90^\circ$ .

Stress concentration at the end of the central guide is more severe in the case of  $\phi = 120^\circ$ , as figures 16 and 17 reveal.

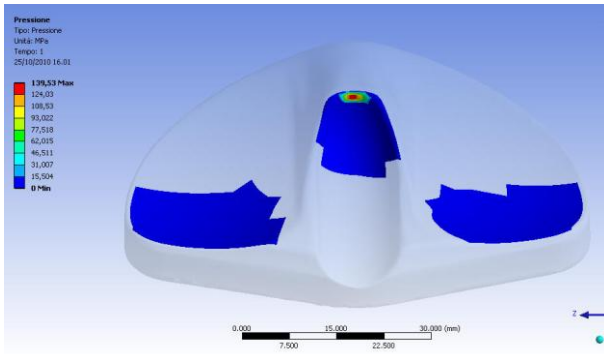


Fig. 16 Contact stress map (Tornier) with  $\phi = 120^\circ$ .

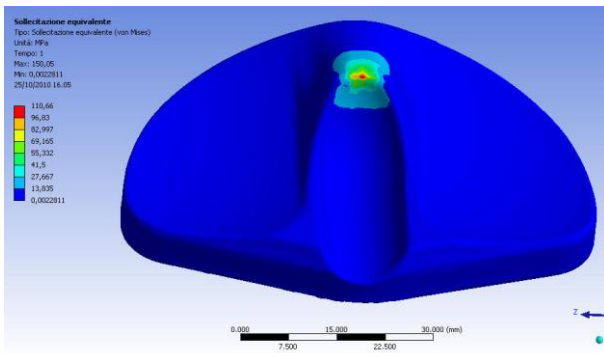


Fig. 17 Von Mises stress map (Tornier) with  $\phi = 120^\circ$ .

### 3.3 FEM results – Comparison of the two prostheses

Results of the analyses previously performed show that the most stressed region of the two prostheses is the central one, both acting as a cam (in the case of Stryker version) or as a guide (in the case of Tornier version). Results obtained for the two joints are collected in the following diagrams in figures 18 and 19, where maximum contact stress and equivalent stress in the PE insert are compared. With the exception of the case of  $\phi = 60^\circ$ , where the central guide of the Tornier prosthesis is unloaded, for the other load cases it is clearly shown that the Stryker prosthesis is subjected to lower stress peaks. This aspect leads to a higher resistance to wearing and static failure of the PE insert.

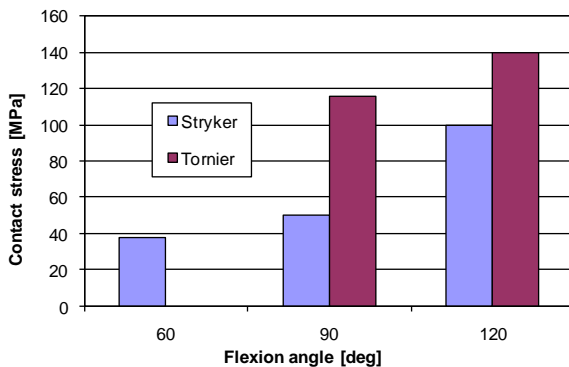


Fig. 18 Maximum contact stress in the PE insert.

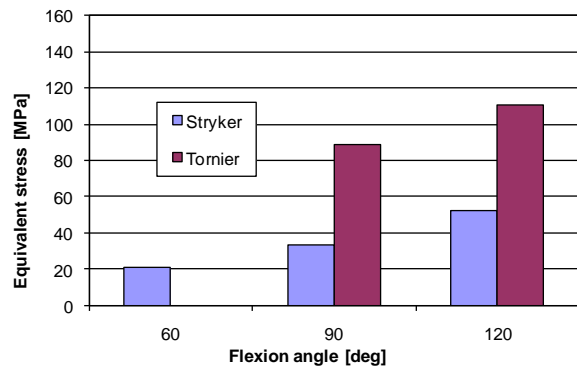


Fig. 19 Maximum Von Mises stress in the PE insert.

### 3.4 FEM results – Improvement of the Stryker prosthesis

In the previous paragraph, it has been proved that, in terms of maximum stresses in the PE insert, the Stryker prosthesis should be preferred with respect to the Tornier one. Starting from the fact that contact stresses depend on the shape of the mating surfaces [9], the central cam of the Stryker joint has been redesigned in order to reduce the peaks of contact stress. In figure 20 a comparison between the original version and the modified one is shown.

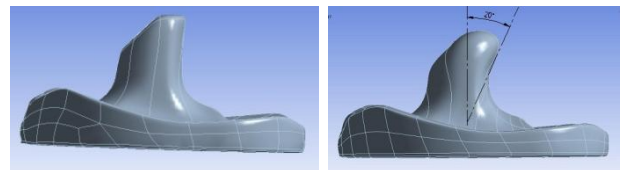


Fig. 20 The original (left) and the modified (right) PE insert of the Stryker prosthesis.

In the original version, the posterior surface of the cam has a tangent plane almost vertical; in the modified version this plane has been rotated up to a value of  $20^\circ$ . This value has been chosen in an arbitrary way, by considering that too low values could have no considerable effect on the results, whereas too high values could obstruct the normal rotations of the knee.

This modification leads to a better distribution of contact without any modification of the kinematics of the joint.

Same load cases have been studied for this modified version of the Stryker prosthesis. Contact and equivalent stress maps obtained are quite similar to those seen for the original Stryker version. What is interesting is the comparison of the maximum stress obtained for the two versions of this prosthesis. Figures 21 and 22 show that the modified Stryker version is characterised by a marked reduction of the peak stress in the case of  $\phi = 120^\circ$  (fig. 23-24), while the other load cases are essentially unchanged.

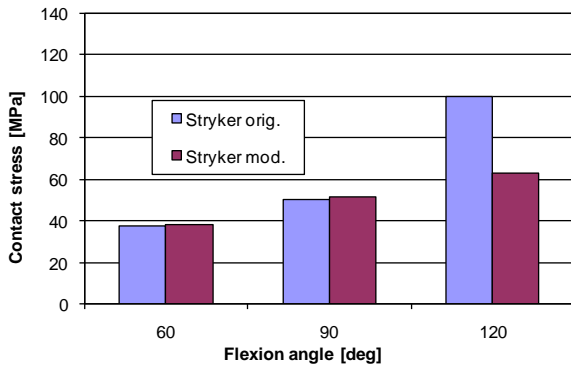


Fig. 21 Maximum contact stress in the PE insert.

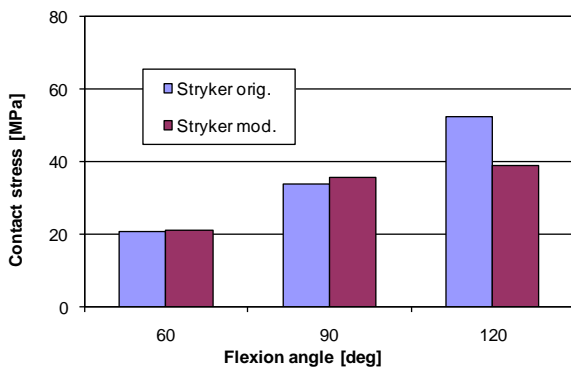


Fig. 22 Maximum Von Mises stress in the PE insert.

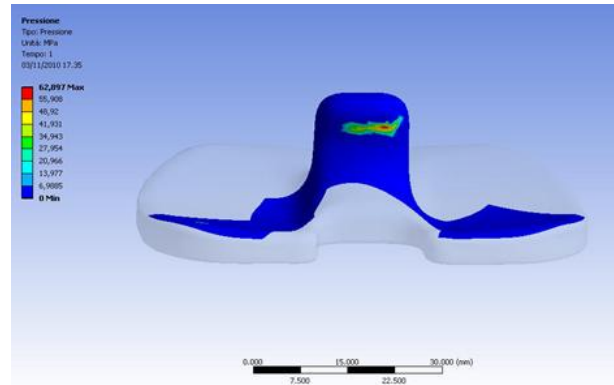


Fig. 23 Contact stress map (Stryker modified) with  $\phi = 120^\circ$ .

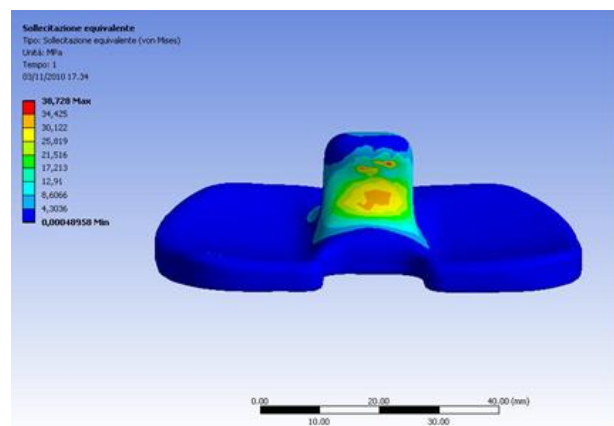


Fig. 24 Von Mises stress map (Stryker modified) with  $\phi = 120^\circ$ .

## 4 Conclusions

In this work a comparison has been performed of the performances of two commercial total knee prostheses, one produced by Stryker and the other by Tornier. Both prostheses are shaped in a way to give posterior stability to the joint, i.e. to avoid joint dislocation under high flexion angles of the knee. Geometries of the prostheses have been acquired via 3D laser scanner techniques. CAD models have been imported into a FEM software where, under some loading and boundary assumptions, contact and equivalent stress fields have been computed. Numerical analyses simulate loading on the joint for different flexion angles.

Results reveal that the Stryker prosthesis is subjected to lower peak stresses; this reduces the risk of wearing of the polyethylene insert and the resultant creation of dangerous debris.

Last step of this work has been the redesign of the Stryker prosthesis in order to enhance its behaviour with high flexion angles. The posterior cam of the PE insert has been reshaped, by giving a different tangent angle of  $20^\circ$ , and smoothed. Lower contact stress peaks have been obtained for this modified version with respect to the original one, without any affection on the kinematics of the original knee joint.

This analysis procedure will be adopted to study different load cases, for example to numerically simulate the case of a complete gait cycle, applying effective loads as the flexion angle varies. Then, considerations about

the wearing and fatigue prediction of the prosthesis during his life-cycle could be done.

## References

- [1] B.C. Carr, T. Goswami, *Knee implants – Review of models and biomechanics*. Materials and Design 30 (2009) pp 398-413.
- [2] T. Nagura, C.O. Dyrby, E.J. Alexander, T.P. Andriacchi. *Mechanical loads at the knee joint during deep flexion*. Journal of Orthopaedic Research 20 (2002) pp 881–886.
- [3] M.Z. Bendjaballah, A. Shirazi-Adl, D.J. Zukor, *Biomechanics of the human knee joint in compression: reconstruction, mesh generation and finite element analysis*. The Knee 2(2) (1995) pp 69-79.
- [4] J.W. Chow. *Knee joint forces during isokinetic knee extensions: a case study*. Clinical Biomechanics 14 (1999) pp 329-338.
- [5] M. Kuster, S. Sakurai, G.A. Wood. *Kinematic and kinetic comparison of downhill and level walking*. Clinical biomechanics 10(2) (1995) pp. 79-84.
- [6] M.S. Kuster, G.A. Wood, G.W. Stachowiak, A. Gachter. *Joint load considerations in total knee replacement*. The Journal of Bone and Joint Surgery. 79-B(1) (1997) pp 109-113.
- [7] W. Mesfar, A. Shirazi-Adl. *Biomechanics of the knee joint in flexion under various quadriceps forces*. The Knee 12 (2005) pp 424-434.
- [8] A. Thambyah. *Contact stresses in both compartments of the tibiofemoral joint are similar even when larger forces are applied to the medial compartment*. The Knee 14 (2007) pp 336–338.
- [9] C-H Huang, J-J Liao, C-H Huang, C-K Cheng. *Influence of Post-cam Design on Stresses on Posterior-stabilized Tibial Posts*. Clinical Orthopaedics And Related Research 450 (2006) pp 150-156.
- [10] H. Bougherara, Z. Mahboob, M. Miric, M. Youssef. *Finite Element Investigation of Hybrid and Conventional Knee Implants*. International Journal of Engineering 3(3) (2009) pp 257-266.
- [11] A.C. Godest, M. Beaugonin, E. Haug, M. Taylor, P.J. Gregson. *Simulation of a knee joint replacement during a gait cycle using explicit finite element analysis*. Journal of Biomechanics 35 (2002) pp. 267–275.
- [12] F. Chen, G.M. Brown, M. Song. *Overview of three-dimensional shape measurement using optical methods*, Optical Engineering 39(1) (2000) pp 10-22.